

FDSPC: Fast and Direct Smooth Path Planning via Continuous Curvature Integration

Zong Chen, and Yiqun Li*

Abstract—In recent decades, global path planning of robot has seen significant advancements. Both heuristic search-based methods and probability sampling-based methods have shown capabilities to find feasible solutions in complex scenarios. However, mainstream global path planning algorithms often produce paths with bends, requiring additional smoothing post-processing. In this work, we propose a fast and direct path planning method based on continuous curvature integration. This method ensures path feasibility while directly generating global smooth paths with constant velocity, thus eliminating the need for post-path-smoothing. Furthermore, we compare the proposed method with existing approaches in terms of solution time, path length, memory usage, and smoothness under multiple scenarios. The proposed method is vastly superior to the average performance of state-of-the-art (SOTA) methods, especially in terms of the self-defined S_2 smoothness (mean angle of steering). These results demonstrate the effectiveness and superiority of our approach in several representative environments.

Index Terms—Motion and path planning, planning under uncertainty, collision avoidance

I. INTRODUCTION

GLOBAL path planning algorithms have undergone significant development in recent years, and played crucial roles in various fields such as autonomous vehicles, robotic arms and unmanned aerial vehicles. However, existing commonly used path planning methods, such as search-based algorithms A* [1], Dijkstra [2], sampling-based algorithms Rapidly-exploring Random Trees (RRT) [3], RRT* [4], extended-RRT [5], and swarm intelligence-based algorithms Ant Colony Optimization (ACO) [6], all yield non-continuous, zigzag global paths. All of these methods also necessitate additional smoothing post-processing, such as polynomial interpolation [7], to be effectively applied in trajectory tracking. Moreover, during the smoothing process, the newly generated path will inevitably deviate from the original collision-free path in certain regions, resulting in additional computational costs.

In this letter, a fast online asymptotically and direct smooth path planning method via curvature integration (FDSPC) is proposed for navigating in unknown environments. The algorithm operates in continuous space versus grid-based or lattice-based planning algorithms, exploring towards the target point

This work was supported in part by the National Natural Science Foundation of China No. 51905185, National Postdoctoral Program for Innovative Talents No. BX20180109.

Authors are with the State Key Laboratory of Intelligent Manufacturing Equipment and Technology, School of Mechanical Science and Engineering, Huazhong University of Science and Technology, Wuhan, 430074, China. (e-mail: liyiqun@hust.edu.cn).

*The implementation of this work is available at https://github.com/SkelonChan/GPCC_curvature_planning.

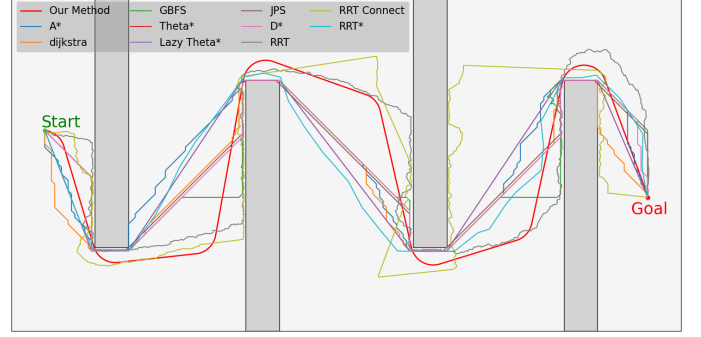


Fig. 1. Comparison of the results of our proposed FDSPC algorithm with other state-of-the-art path planning algorithms in simple maze.

iteratively to find collision-free path segments that satisfy G^2 smoothness (curvature continuity), eventually constructing a complete path. In this algorithm's data structure, a variant of the direct positioning binary tree combined with an ordered dictionary is constructed, enabling fast heuristic search of the path and ensuring both the feasibility and efficiency of the algorithm. The planning algorithm automatically reverts to the previous optimal solution when trapped in local solution by backtracking, and prunes tree nodes associated with local solutions to maintain the feasibility of global solution. Additionally, by employing continuous curvature for path planning, any curve can be represented solely by its curvature variation function. With known FDSPC parameters, the algorithm can subsequently compute the pose (x, y, θ) of the curve, which significantly reduces bandwidth during path transmission.

Compared to existing classical and SOTA methods, FDSPC can generate a global smooth path satisfying G^2 continuity without smoothing process, as illustrated in Fig. 1. This eliminates the need for subsequent re-collision checking and smoothing. The proposed method consistently demonstrates superior performances by comparing and evaluating various indicators, including CPU time, memory, smoothness, in multiple representative scenarios. The contributions of this letter are as follows:

- 1) An online fast global path planning method based on continuous curvature integration is proposed, which can generate global paths that satisfies G^2 smoothness, avoiding the re-collision checking and extra path smoothing.
- 2) A variant of the direct positioning binary tree combined with an ordered dictionary is introduced to facilitate heuristic search of the path rapidly and ensuring both the feasibility and efficiency of the algorithm.

- 3) A variety of evaluation indicators in multiple scenarios are compared, and the proposed method consistently demonstrate extraordinary performances.

II. RELATED WORKS

A. Classical path planning

The path planning problem has been around for decades, and the methods can be divided into two categories, i.e., search-based approach and sampling-based approach. The search-based approach usually discretizes the unknown environment and searches for the optimal path in the grid map. Besides, the resolution of the grid map affects the accuracy and efficiency of the algorithm directly.

Search-based A* can quickly find the asymptotically optimal path through the heuristic function. Dijkstra's algorithm could find the global optimal solution, but its time complexity is high. The sampling-based methods are to sample in the configuration space and then find a feasible path through the sampling points. RRT, RRT* and Bidirectional Hybrid Safety Certificate (BiHSC) [8] can adapt well in high-dimensional space and complex environment, but can not guarantee to find the optimal solution, and the planned paths are often zigzag. RRT-connect [9] satisfies the completeness, but often owns low convergence rate. Extended-RRT combines the nonholonomic constraints of the robots, but exhibits low computation efficiency. Mostly, the paths generated by swarm intelligence optimization [10], [11] are more prone into local optimum. The optimization-based methods [12], [13] minimize the pre-defined cost function under various constraints, which requires a good initial value of iteration, otherwise the time efficiency and feasibility are difficult to guarantee.

B. Smooth path planning

Building upon the preceding path results, the curve planning method is crafted by amalgamating pathfinding and smoothness through the incorporation of Reed-Shepp (RS) curves [14], Bezier curves, or similar techniques. The hybrid A* algorithm [15] transmutes the discrete grid map space into a continuous space and smooths the A*-derived path using RS curves. This ensures that the planned curve adheres to the vehicle's kinematic constraints and achieves G^1 continuity (Tangent continuity), resulting in excellent tracking performance. However, additional optimization processes are still required for the final trajectory. [16], [17] propose a hierarchical search spatial scales-based hybrid A* (HHA*) framework, employing clothoids instead of RS curves, thereby attaining G^2 continuity in the path and exhibiting commendable performance in parking scenarios. [18], [19] design a continuity curvature constraint as a local path planner embedded within the global path planner, resulting in collision-free and smooth paths.

Clothoids with continuous curvature expand the original motion primitive and enhance the granularity of the search space. However, clothoids are defined in terms of Fresnel integrals [20], making them challenging to be applied online. To address this, a lookup table is constructed to store the coordinates of basic clothoids [21], which accelerates calculations when dealing with other clothoids, yielding lower errors

compared to approximations using Bézier or B-spline curves [22]. Nevertheless, achieving an exact approximation for the clothoid is not the most crucial for path planning, especially in iterative approaches, and none of the aforementioned algorithms generate a smooth, globally applicable path or trajectory directly and rapidly.

In this letter, a fast and direct path planning method FDSPC with G^2 continuity without extra smoothing is proposed.

III. CURVATURE PLANNING

A. Curvature planning analysis

A succinct representation of a path in n -dimensional (n -D) space can be expressed as the set \mathcal{C} of coordinates of discrete points $p \in \mathbb{R}^n$. The direction and curvature of the path can be indirectly calculated from the point set \mathcal{C} , but significant errors often arise due to the discontinuity of the waypoints. Typically, interpolation of discrete points is required for obtaining a smoother representation of the path. For any curve in n -D space, it can be precisely described by a function of $n - 1$ D. For example, in a 2-D plane, the curve can be described by a 1-D curvature κ , while in 3-D space, both the curvature κ and the z -direction scaling function τ can be used.

The ultimate goal of the robot path planning is to find a smooth curve that connects the start point and the end point in an unknown environment as quickly and concisely as possible. A curvature planning function $\hat{f}(\kappa) = \rho$ is introduced, which ensures G^2 continuity through the continuous curvature integration and meets the smoothness requirement. Search speed is accelerated by incorporating heuristic weight and two-tiered search-based exploration. Global feasibility of the proposed algorithm is ensured by the introduction of a backtracking mechanism, enabling the algorithm to revert to the previous optimal solution when trapped in local optima. The smooth extension of the path towards the end point is facilitated through pruning operations.

B. Curvature planning in 2-D space

The relative positional relationship between path points in 2-D and the obstacles is not directly discernible through the implicit expression of curvature planning. Thus, it is necessary to explicitly unfold the implicit expression, i.e., curvature function κ , of the path in 2-D space. By double integrating the κ , path point information is obtained to evaluate the planning feasibility and adjust the curvature accordingly. The relationship between curvature and the tangent at the path points can be expressed as,

$$\frac{d\theta}{ds} = \kappa \Rightarrow \frac{d\theta}{dt} \frac{dt}{ds} = \kappa \Rightarrow \frac{d\theta}{dt} = \kappa \frac{ds}{dt} \quad (1)$$

where θ is the tangent angle of the path, s is the arc length of the path, dt is the integration step of the path, κ is the path curvature, and ds/dt can be regarded as the pseudo speed of the path (the rate of change of distance along the curve). The tangent angle function $\theta(t)$ of the path can be obtained by integrating the curvature function $\kappa(t)$ and the pseudo speed ds/dt .

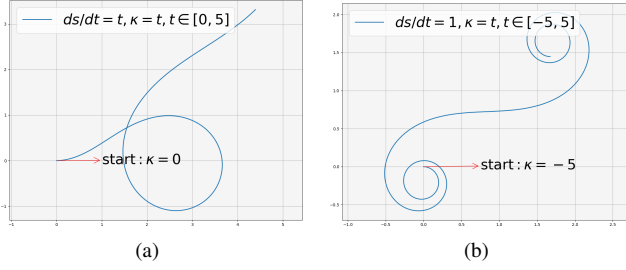


Fig. 2. The demonstration of the evolution of the curvature planning model under different curvature functions.

The model of the curvature path planning can be expressed as,

$$\begin{aligned}
 \dot{\kappa} &= \rho \\
 \dot{v} &= a \\
 \dot{\theta} &= \kappa \cdot \frac{ds}{dt} \\
 \dot{x} &= \frac{ds}{dt} \cdot \cos(\theta) \\
 \dot{y} &= \frac{ds}{dt} \cdot \sin(\theta)
 \end{aligned} \tag{2}$$

where ρ represent the rate of change of curvature, a represent the pseudo acceleration along the curve.

If we set ds/dt to be constant 1, the waypoints can be strictly expressed as trigonometric functions with respect to the curvature, and the equation 2 can be expressed as,

$$\begin{aligned}
 \dot{\kappa} &= \rho \\
 \dot{\theta} &= \kappa \\
 \dot{x} &= \cos(\theta) \\
 \dot{y} &= \sin(\theta)
 \end{aligned} \tag{3}$$

Through equation 3, the relationship between the path described by the curvature κ and the obstacles can be established. Subsequently, the positions of provisional path points can be derived by integration, and examine whether these path points collide with the obstacles. If collisions occur, adjust the curvature κ accordingly. This iterative process ensures that FDSPC obtains a curvature description of the path that maintains G^2 continuity while avoiding collisions with obstacles. The evolution of the curvature planning model under different curvature functions is demonstrated in Fig. 2.

IV. FDSPC ALGORITHM

A. Data structure

Any obstacle encountered during the search in the plane, it can be avoided by circling on the left or right side. Therefore, if each encountered obstacle is viewed as a node of a binary tree, the path search process can be regarded as the construction of a binary tree from the root node (initial position) to the leaf nodes (target position). Each binary tree node stores path information or curvature information from the previous node to the current node, the node's search weight (the Euclidean distance from the current node position to the end point position) and the node's location information (the node's position in the binary tree) is stored in an ordered

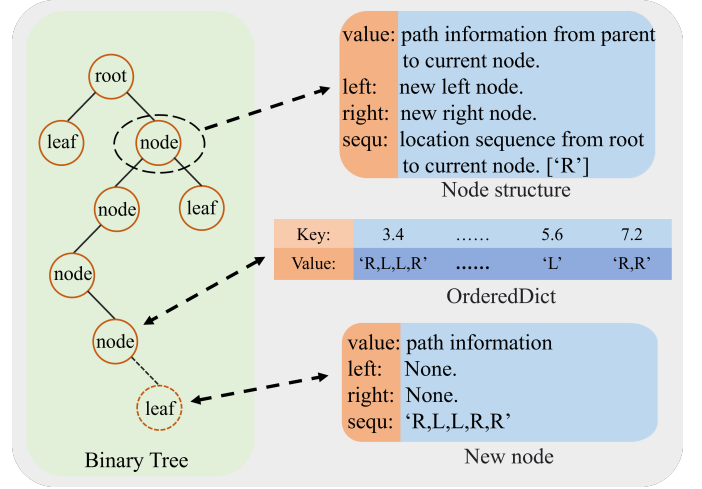


Fig. 3. The data structure of the FDSPC algorithm.

dictionary. Whenever there arises a necessity to update and broaden potential path nodes, the location information of the node with the lowest weight is popped out from the ordered dictionary. This enables rapid localization of the node to be expanded in the binary tree, thus achieving rapid heuristic search of the path. The data structure framework of the FDSPC algorithm is illustrated in Fig. 3.

The path begins with the initialization of the root node in the binary tree, and the destination is marked as the leaf node. Each node in the binary tree holds the *value*, representing the path information from the preceding node to the current node. Additionally, the sequence (*right* or *left*) stored in the *sequ* attribute indicates the locating sequence in the binary tree from the root node to the current node. A corresponding node is created in the binary tree, when a new obstacle is encountered,. This involves expanding either the left subtree or the right subtree, depending on the node's direction. This iterative process persists until the target position is attained. During the expansion of child nodes, the Euclidean distance from the current position to the end point position is used as the *key* (also regarded as the weight of node selection), simultaneously, the locating sequence from the root node (starting position) to the current node (current position) of the binary tree is viewed as the *value*. They are paired and added to the ordered dictionary. This arrangement facilitates rapid retrieval of the nearest node and fast localization of potential update nodes. After adding a new node, pruning the parent nodes in the ordered dictionary where both left and right child nodes exist (indicating infeasibility of both left and right expansions). This step ensures that only expandable node information remains in the ordered dictionary, thereby reducing redundant searches.

B. Smooth path planning

The initialization of the FDSPC algorithm is illustrated in Alg. 1. Firstly, the algorithm checks whether the current orientation enables a direct reach to the end point (i.e., if there is no obstacle along a straight line path from current position to the end point). If not, it proceeds to iteratively adjust the

Algorithm 1: Direct planning $D_p(\cdot)$

```

1 Initialize  $\theta_g \leftarrow \arctan 2(p_{start}, p_{goal})$ 
2 if  $\theta_g \neq \theta_0$  then
3   while True do
4      $\kappa_{s1} \leftarrow \int \rho$ 
5      $\theta \leftarrow \int \kappa_{s1}$ 
6     update  $p_{now}$ 
7      $\theta_g \leftarrow \arctan 2(p_{now}, p_{goal})$ 
8     if  $\theta = \theta_g$  then
9       break
10    end
11  end
12 end
13  $\kappa_{s2} \leftarrow \mathbf{0}$ 
14  $\kappa_d \leftarrow \kappa_{s1} + \kappa_{s2}$ 
15 return  $\kappa_d$ 

```

current orientation θ using the curvature integral until the direction of the line connecting the current position and the end point aligns with the current orientation. Subsequently, by assigning a curvature value of 0 to the straight-line segment, it sequentially connects the current position to the end point, ensuring the path that maintains G^2 continuity. Essentially, the FDSPC algorithm constructs the basic path structure by combining segments of indefinite radius arcs with straight lines.

Algorithm 2: Explore planning $E_p(\cdot)$

```

1 Initialize  $\theta_t, \theta_0 \leftarrow \arctan 2(p_{now}, p_{goal})$ ;
2 Initialize  $\kappa_s \leftarrow \mathbf{0}$ ;
3 Initialize  $o_{idx} \leftarrow \mathcal{O}_d(\mathcal{F}_{map}, \kappa_s)$ ;
4 while  $o_{idx}$  is not empty and  $|\theta_t - \theta_0| < \pi$  do
5   while  $o_{idx}$  is not empty do
6      $\kappa_{old} = \kappa_s, o_{idx,old} = o_{idx}$ ;
7      $len_{int} = o_{idx} + len_{add}$ ;
8      $\theta_t = \theta_t \pm \theta_{a1}$ ;
9      $\kappa_s \leftarrow \int_{inv}(\theta_t, \rho, len_{int})$ ;
10     $o_{idx} \leftarrow \mathcal{O}_d(\mathcal{F}_{map}, \kappa)$ ;
11  end
12  if  $\theta_{a1} == \theta_{a2}$  then
13    break;
14  end
15   $\theta_t = \theta_t \mp \theta_{a1}$ ;
16   $\kappa_s = \kappa_{old}$ ;
17   $\theta_{a1} = \theta_{a2}$ ;
18 end
19  $\kappa_a \leftarrow P_{fimin}(\kappa_{old}[o_{idx,old}], \kappa_s)$ ;
20 return  $\kappa_a$ ;

```

The direct planning function $D_p(\cdot)$ encounters collision issues easily when initialized in environments with obstacles. To address this, an exploration function $E_p(\cdot)$ is introduced, which navigates around obstacles by altering the current orientation θ . The detailed implementation of the exploration function is illustrated in Alg. 2.

Algorithm 3: FDSPC

```

1 Initialize  $\kappa_d \leftarrow D_p(p_{start}, p_{goal}, \theta_0)$ ;
2 Initialize  $obs_{idx} \leftarrow \mathcal{O}_d(\mathcal{F}_{map}, \kappa_d)$ ;
3 update  $p_{now}, \mathcal{B}_t(p_{now}), \mathcal{O}_d(p_{now})$ ;
4 while  $obs_{idx}$  is not empty do
5    $\kappa_a \leftarrow E_p(\mathcal{F}_{map}, p_{now}, p_{goal})$ ;
6   update  $p_{now}, \mathcal{B}_t(p_{now}), \mathcal{O}_d(p_{now})$ ;
7    $\kappa_d \leftarrow D_p(p_{start}, p_{goal}, \theta_0)$ ;
8    $obs_{idx} \leftarrow \mathcal{O}_d(\mathcal{F}_{map}, \kappa_d)$ ;
9   update  $p_{now}, \mathcal{B}_t(p_{now}), \mathcal{O}_d(p_{now})$ ;
10 end
11  $\kappa \leftarrow \mathcal{B}_t$ ;
12 return  $\kappa$ ;

```

The algorithm initially endeavors to establish a connection between the current position and the end point along the current orientation θ using a straight line, and calculates the position index of the collision point. If the index is non-empty and the added extension angle is less than π , it progressively increases the extension angle θ_t on both sides of the obstacle until the index of the collision point become empty. The integration exploration length len_{int} is adjusted based on the position index of the collision point o_{idx} by adding a length len_{add} to avoid overly long exploration distances that might mistakenly identify boundaries as obstacles, rendering the problem unsolvable. In line 9 of Alg. 2, a sequence κ_s of curvatures is obtained through reverse integration under specified integration length len_{int} , integral value θ_t , and integration rate ρ . Upon the program runs into the inner while loop (line 5 to line 11, Alg. 2) for the second time, the added extension angle begins increasing from the previous collision angle by increments of θ_{a2} ($\theta_{a2} < \theta_{a1}$) to refine the exploration of collision edges until the position index of the collision point is empty and exiting the while loop. Finally, the algorithm utilizes the $P_{fimin}(\cdot)$ function to locate a point a on the current collision-free curvature path κ_s that minimizes the distance to the previous collision position on the curvature path κ_{old} . Subsequently, the algorithm returns the collision-free curvature path κ_a preceding point a on κ_s .

In Alg. 2, if the added angle to both sides, i.e., $|\theta_t - \theta_0|$, exceeds π , the exploration node is manually closed. This involves pruning the extra nodes, and subsequently, a new node is popped from the binary tree \mathcal{B}_t .

Alg. 3 outlines the overall framework of the FDSPC algorithm. Initially, the algorithm procures an initial curvature path κ_d via the direct planning function $D_p(\cdot)$. Subsequently, the collision detection function $\mathcal{O}_d(\cdot)$ is employed to assess the feasibility of the path. In case of collision detection, the algorithm retraces its steps along the collision point sequence by a length of $back_{obs}$ to identify a branch point b . It then incorporates this branch point along with the collision-free branching path into the binary tree \mathcal{B}_t and the ordered dictionary $\mathcal{O}_d(\cdot)$. Using the exploration function $E_p(\cdot)$, a short collision-free curvature path κ_a is obtained, \mathcal{B}_t and $\mathcal{O}_d(\cdot)$ are updated accordingly. The algorithm proceeds to iterate through the direct planning function $D_p(\cdot)$ once more to derive a new

TABLE I
PARAMETERS OF FDSPC MOTION PLANNING

Symbol	Description	Value	Unit
dt	The step of curvature integral	0.01	s
$back_{obs}$	Collision setback distance	0.8	m
θ_{a1}	First time exploring added angles	0.1	deg
θ_{a2}	Second time exploring added angles	0.01	deg
len_{add}	Post-collision 2nd scan add length	0.5	m
κ_{limit}	Maximum absolute value of κ	2.5	deg/m
$\dot{\kappa}_{limit}$	Maximum absolute value of $\dot{\kappa}$	40	deg/m-s
θ_0	The initial θ at the start point	0	deg
κ_0	The κ value in a straight line	0	deg/m

curvature path κ_d , repeating this cycle until a collision-free curvature path κ_d is found. Finally, the algorithm traverses the branches of the binary tree \mathcal{B}_t in reverse order from the end point leaf to obtain the final curvature path κ .

The algorithm selects the position of the node with the smallest weight in the popped binary tree based on the *key* of the ordered dictionary for subsequent expansion. The integration length len_{int} is initially set as the Euclidean distance between the current position p_{now} and the end point p_{goal} , and it is further adjusted based on the collision position index o_{idx} . During planning in proximity to obstacles, after updating the collision point, the newly added node often coincides with the position of the last expansion node, as depicted in the subfigure of Fig. 4(b). This scenario poses a risk of generating pseudo-feasible paths where all newly added paths are collision-free within the specified expansion length but do not reach the end point, and this situation can potentially lead to premature termination of the algorithm. To mitigate this issue, for pseudo-feasible paths encountered in Alg. 2, we opt to select a small initial segment and continue planning from the new node position. In essence, the FDSPC algorithm must commence and conclude with Direct planning $D_p(\cdot)$, interspersing Explore planning $E_p(\cdot)$ in between.

The parameters of the FDSPC algorithm are shown in Table I.

V. SIMULATION AND ANALYSIS

In this section, we validate the FDSPC algorithm through simulations. Five typical scenarios are tested and the performance of FDSPC algorithm with state-of-the-art methods [23] in the same environment are compared. All experiments are conducted on a PC with an AMD Ryzen 5 5600X CPU @ 3.7GHz and 32 GB RAM.

A. Simulation results

In the verification, five typical scenarios are crafted designed, including bypassing long obstacles, navigating through long corridors and semi-enclosed areas, traversing random complex and simple maze environments. The specific implementation process and the final feasible smooth path are shown in Fig. 4.

In the scenario of bypassing long obstacles, the algorithm successfully discovers a short and smooth path by maneuvering closer to the edge of the obstacle. In the long corridor, random complex and simple maze scenarios, the FDSPC

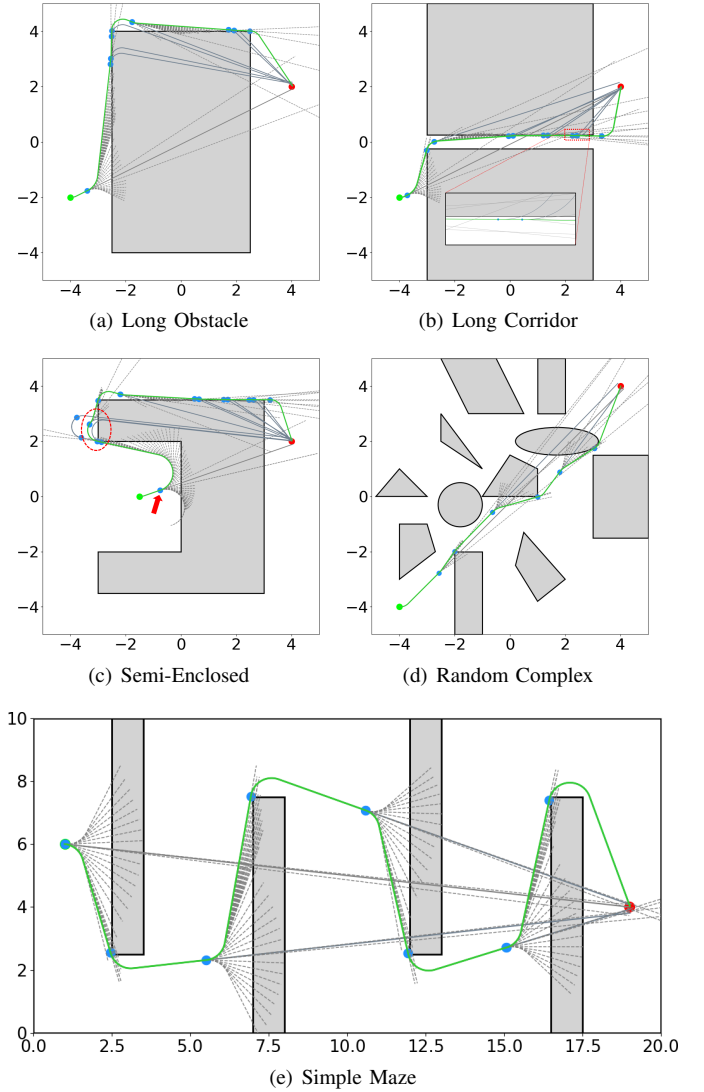


Fig. 4. Simulation processions and results of the FDSPC algorithm in long obstacle (a), long corridor (b), semi-enclosed (c), random complex (d) and simple maze (e) scenarios. The light gray area represents the obstacle area, the blue dots indicate branch nodes added to the binary tree. The gray dashed line, the green line and the dodger blue line indicate the probe length of the Explore planning function, the final feasible path and the direction planning path, respectively. The initial and final position are marked with a red and lime dot, respectively. (a) : $(x_0, y_0) = (-4, -2)$, $(x_f, y_f) = (4, 2)$, (b) : $(x_0, y_0) = (-4, -2)$, $(x_f, y_f) = (4, 2)$, (c) : $(x_0, y_0) = (-1.5, 0)$, $(x_f, y_f) = (4, 2)$, (d) : $(x_0, y_0) = (-4, -4)$, $(x_f, y_f) = (4, 4)$, (e) : $(x_0, y_0) = (1, 6)$, $(x_f, y_f) = (19, 4)$. In (e), $\kappa_{lim} = 1.5$, $\dot{\kappa}_{limit} = 20$, $back_{obs} = 1.5$. Video explanation and the simulation process can be found at https://github.com/SkelonChan/GPCC_curvature_planning.

algorithm, aided by the heuristic function, adeptly identifies a smooth path satisfying G^2 continuity, as shown in Fig. 4(a), 4(b), 4(d), and 4(e). In the semi-enclosed scenario, the FDSPC algorithm extends branches to both sides of the obstacle, determining that the feasible shortest path needs to pass from the left side, and adds collision-free branch points to the binary tree, as indicated by the red circle in Fig. 4(c). When popping a new node from the ordered dictionary, since the newly expanded node in the red circle is farther from the end point, it has a higher weight. Consequently, the algorithm prioritizes

updates from the unexpanded direction (right) of the first node (pointed by the red arrow). If the expansion angle exceeds π and no new node is found, the node is pruned, and a new node is popped for subsequent planning. Throughout these scenarios, more or less pseudo-feasible paths are encountered. Extending these pseudo-feasible paths in small segments, (as shown by the two adjacent blue points in Fig. 4(b) and 4(c)), the algorithm ultimately achieves successful discovery of feasible smooth paths.

B. Performance analysis

To ensure comparability among the algorithms in the comparative experiments, the parameters are standardized in the following manner:

- 1) For grid-based algorithms such as A*, the resolution of the grid map is set to 0.01 to match the dt resolution of the FDSPC algorithm.
- 2) For probabilistic sampling-based algorithms such as RRT, the maximum number of samples is capped at 15000, and the maximum extension step length is set to 0.05. Setting the step length to 0.01 might impede the algorithm's convergence.

The FDSPC algorithm with 10 other algorithms in terms of path-solving time, memory usage, path length, and path smoothness (\mathcal{S}_1 and \mathcal{S}_2) are compared in five typical scenarios, i.e., long obstacles, long corridors, semi-enclosed areas, random complex and simple mazes scenarios. The comparative results are presented in Fig. 5, 6, 7, 8 and 9. The path-solving time and memory usage are measured using the Python 'time' library and 'psutil' library, respectively. Path length is calculated based on the Euclidean distance between discrete points, while the path smoothness (\mathcal{S}_1 and \mathcal{S}_2) are computed using the formulas presented in Equations 4 and 5.

\mathcal{S}_1 is defined as the average change in heading per unit length along the path, which is defined as follows,

$$\mathcal{S}_1 = \frac{\sum_{i=1}^{n-1} \theta_i}{l_p}$$

$$\theta_i = \begin{cases} \arccos\left(\frac{\vec{p_{i-1}p_i} \cdot \vec{p_i p_{i+1}}}{|p_{i-1}p_i| \cdot |p_i p_{i+1}|}\right), & |p_{i-1}p_i| \cdot |p_i p_{i+1}| \neq 0 \\ 0, & \text{otherwise} \end{cases} \quad (4)$$

where, l_p is the path length, p_i is the point coordinate of the path, and n is the number of path points.

However, the average change in heading per unit length \mathcal{S}_1 may not objectively and accurately evaluate the smoothness of the entire path. For algorithms like Jump Point Search (JPS), the generated path comprises only a few discrete waypoints connected by straight lines, lead to high smoothness in terms of \mathcal{S}_1 . However, abrupt changes or even sharp turns may occur at these waypoints, leading to poor overall path smoothness. Therefore, the smoothness measurement \mathcal{S}_2 is introduced, which is defined as the mean angle of turning. It is defined as

follows,

$$\mathcal{S}_2 = \frac{\sum_{i=1}^{n-1} \theta_i}{l_c}$$

$$\theta_i = \begin{cases} \arccos\left(\frac{\vec{p_{i-1}p_i} \cdot \vec{p_i p_{i+1}}}{|p_{i-1}p_i| \cdot |p_i p_{i+1}|}\right), & |p_{i-1}p_i| \cdot |p_i p_{i+1}| \neq 0 \\ 0, & \text{otherwise} \end{cases} \quad (5)$$

where, l_c is the number of θ_i that is not 0.

In the five scenarios, the solving time and memory usage of each algorithm are depicted in Fig. 5 and Fig. 6 respectively. Thanks to its exploration of feasible trajectories through angle extensions, FDSPC exhibits higher solving speed compared to point-to-point planning algorithms like A* based on grid maps. Although the solving time of FDSPC may not be the shortest, it still ranks among the fastest algorithms. Moreover, unlike algorithms such as RRT based on random sampling, FDSPC demonstrates stable solving times in all scenarios without significant fluctuations. Regarding memory usage, all algorithms employ the Python Matplotlib visualization library for collision detection, leading to relatively high overall memory usage. However, the memory usage of FDSPC is slightly lower than the average. In simulations, FDSPC involves numerous integration processes to explore potential collision-free paths. However, in practical applications, sensors such as LiDAR and depth cameras can directly provide distance information in a given direction, avoiding the need for extensive integration operations. Consequently, FDSPC's actual memory usage and solving time can be further reduced.

In terms of path length, the FDSPC algorithm generally performs at an average level in all scenarios. However, in the semi-enclosed scenario, the FDSPC algorithm exhibits a significant increase. This can be attributed to the additional θ dimension introduced by the FDSPC algorithm compared to others, and the substantial deviation between the initial orientation and the feasible path orientation, that causes the FDSPC algorithm bypasses through nearly 180 degrees, giving rise to a notable increase in path length.

Fig. 8 and Fig. 9 depict the comparison of path smoothness \mathcal{S}_1 and \mathcal{S}_2 among different algorithms. Regarding \mathcal{S}_1 smoothness, the FDSPC algorithm consistently ranks among the top performers in all scenarios, slightly surpassing θ^* , lazy θ^* , and aligning with algorithms like JPS, achieving only about one-fifth of the average level. In the comparison of \mathcal{S}_2 smoothness, the FDSPC algorithm significantly outperforms others due to its utilization of curvature-based planning. The \mathcal{S}_2 smoothness of FDSPC is vastly superior to the average level, being enhanced by two orders of magnitude.

VI. CONCLUSION

In this paper, we introduced a novel path planning algorithm, FDSPC, based on continuous curvature integration. The algorithm explores feasible paths through continuous transformations of curvature angles, offering advantages such as high solution speed, efficient memory usage, shorter path lengths and exceptional path smoothness. The paths generated by the algorithm can be directly tracked as trajectories with a constant velocity. In five typical scenarios, the FDSPC

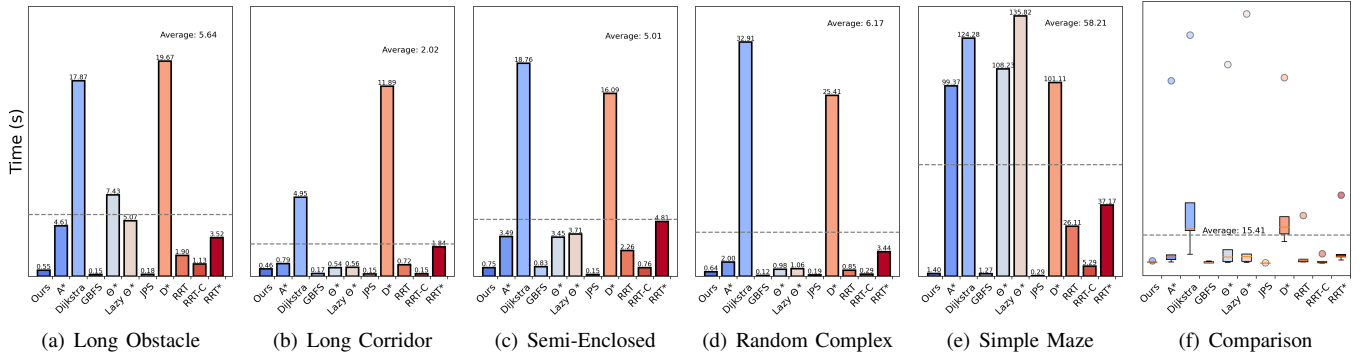


Fig. 5. (a)-(e) show the comparison of path solving time between the FDSPC algorithm and others in different maps with the same constraint condition. (f) shows the comparison of the data box-plots in five scenarios. And the gray dashed line is the mean of the solution time of all algorithms in this scenario.

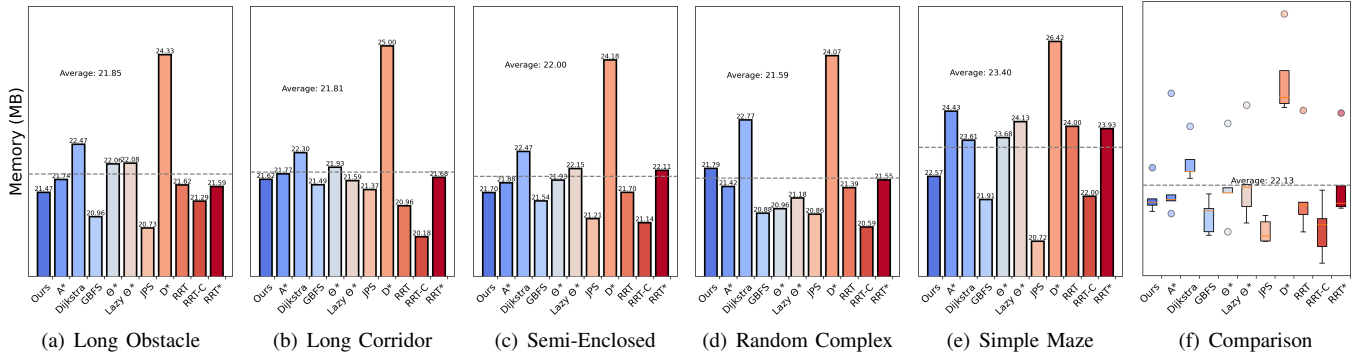


Fig. 6. (a)-(e) show the comparison of memory usage between the FDSPC algorithm and others in different maps with the same constraint condition. (f) shows the comparison of the data box-plots in five scenarios. And the gray dashed line is the mean of the memory usage of all algorithms in this scenario.

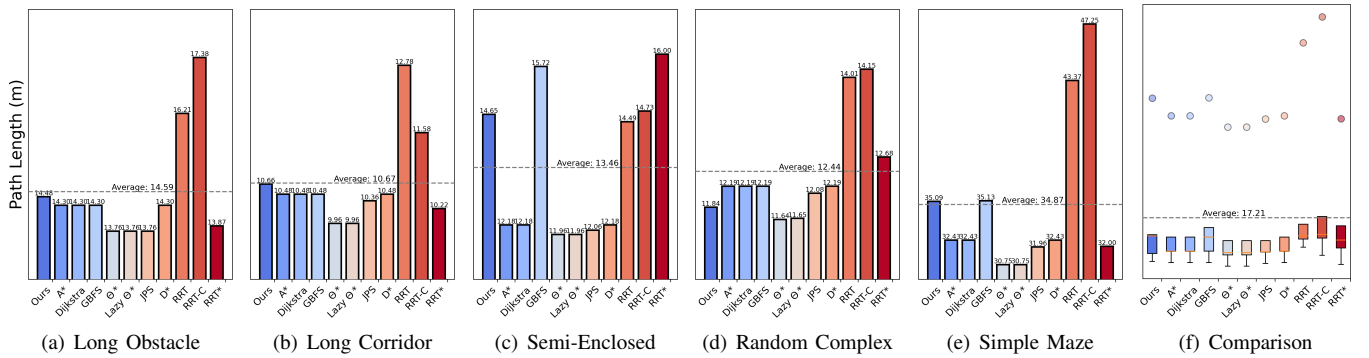


Fig. 7. (a)-(e) show the comparison of path length between the FDSPC algorithm and others in different maps with the same constraint condition. (f) shows the comparison of the data box-plots in five scenarios. And the gray dashed line is the mean of path length of all algorithms in this scenario.

algorithm consistently demonstrated superior performance in long obstacle bypass, long corridor, semi-enclosed, random complex and simple maze scenarios. However, FDSPC also exhibits several drawbacks. For instance, it requires adjustments to some tunable parameters in complex or extreme scenarios. In practical applications, the use of sensors such as LiDAR and depth cameras can mitigate the need for extensive integration, further reducing memory usage and solution time.

In the future, we will focus on further optimizing the FDSPC algorithm to enhance its robustness, streamline the number of adjustable parameters, improve its completeness, and augment its adaptability to a broader spectrum of com-

plex scenarios. Moreover, given that the model represented by Equation 2 can be regarded as a simplified kinematic model, and optimization-based approaches to directly derive the optimal path can be explored. Additionally, compared to other algorithms, FDSPC introduces an additional dimension for path orientation, θ , and demonstrates exceptionally high path smoothness. Hence, we aim to investigate its utility as an initial value for trajectory optimization of mobile robots.

REFERENCES

- [1] P. E. Hart, N. J. Nilsson, and B. Raphael, "A formal basis for the heuristic determination of minimum cost paths," *IEEE Trans. Syst. Sci. Cybern.*, vol. 4, no. 2, pp. 100–107, 1968.

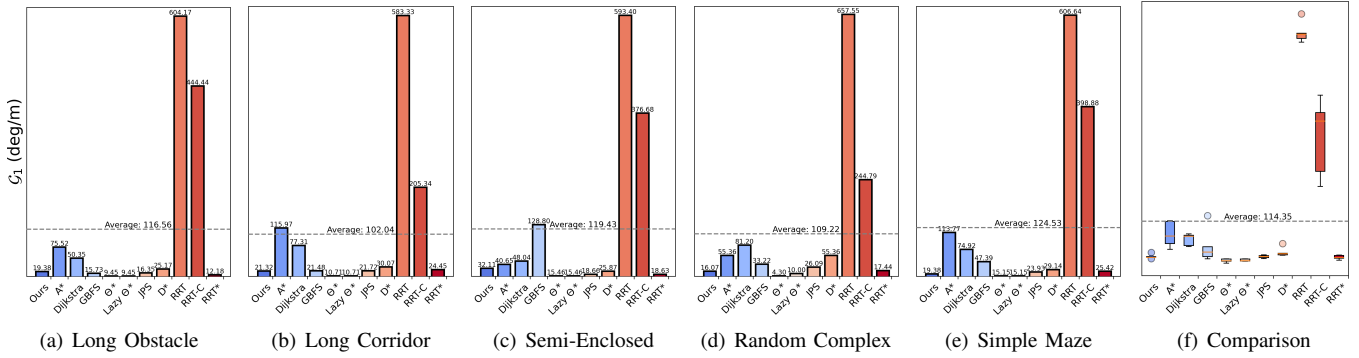


Fig. 8. (a)-(e) show the comparison of path smoothness S_1 between the FDSPC algorithm and others in different maps with the same constraint condition. (f) shows the comparison of the data box-plots in five scenarios. And the gray dashed line is the mean of the S_1 of all algorithms in this scenario.

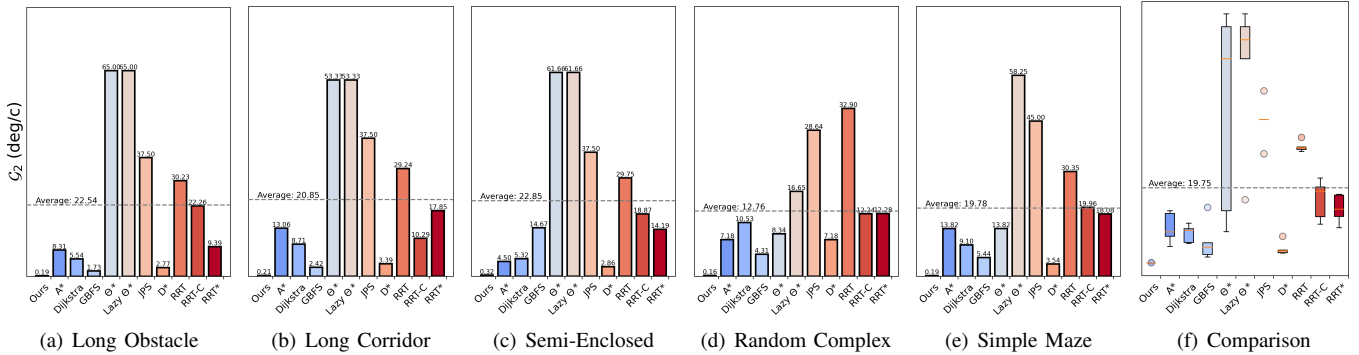


Fig. 9. (a)-(e) show the comparison of path smoothness S_2 between the FDSPC algorithm and others in different maps with the same constraint condition. (f) shows the comparison of the data box-plots in five scenarios. And the gray dashed line is the mean of the S_2 of all algorithms in this scenario.

- [2] E. W. Dijkstra, "A note on two problems in connexion with graphs," *Numerische Mathematik*, vol. 50, pp. 269–271, 1959.
- [3] S. M. LaValle and J. J. Kuffner Jr, "Randomized kinodynamic planning," *Int. J. robot. Res.*, vol. 20, pp. 378–400, 2001.
- [4] S. Karaman and E. Frazzoli, "Incremental sampling-based algorithms for optimal motion planning," *Robot Sci. Syst. VI*, vol. 104, no. 2, pp. 267–274, 2010.
- [5] J. Bruce and M. Veloso, "Real-time randomized path planning for robot navigation," in *Proc. IEEE Int. Conf. Intell. Robots Syst.*, vol. 3, 2002, pp. 2383–2388.
- [6] Y. Chen, G. Bai, Y. Zhan, X. Hu, and J. Liu, "Path planning and obstacle avoiding of the usv based on improved aco-apf hybrid algorithm with adaptive early-warning," *IEEE Access*, vol. 9, pp. 40 728–40 742, 2021.
- [7] Y. Li, Z. Chen, T. Wang, X. Zeng, and Z. Yin, "Apollo: Adaptive polar lattice-based local obstacle avoidance and motion planning for automated vehicles," *Sensors*, vol. 23, no. 4, p. 1813, 2023.
- [8] S. Shi, J. Chen, and Y. Li, "Hybrid safety certificate for fast collision checking in sampling-based motion planning," *IEEE Robot. Autom. Lett.*, vol. 8, no. 1, pp. 113–120, 2022.
- [9] J. J. Kuffner and S. M. LaValle, "Rrt-connect: An efficient approach to single-query path planning," in *Proc. IEEE ICRA. Millennium Conf., Int. Conf. Robot. Automat. Symposia Proc. (Cat. No. 00CH37065)*, 2000, pp. 995–1001.
- [10] W. Shi, Z. He, W. Tang, W. Liu, and Z. Ma, "Path planning of multi-robot systems with boolean specifications based on simulated annealing," *IEEE Robot. Autom. Lett.*, vol. 7, no. 3, pp. 6091–6098, 2022.
- [11] V. Roberge, M. Tarbouchi, and G. Labonté, "Comparison of parallel genetic algorithm and particle swarm optimization for real-time uav path planning," *IEEE Trans. Ind. Informat.*, vol. 9, no. 1, pp. 132–141, 2012.
- [12] Q. Hu, J. Xie, and C. Wang, "Dynamic path planning and trajectory tracking using mpc for satellite with collision avoidance," *ISA Trans.*, vol. 84, pp. 128–141, 2019.
- [13] Z. Zuo, X. Yang, Z. Li, Y. Wang, Q. Han, L. Wang, and X. Luo, "Mpc-based cooperative control strategy of path planning and trajectory tracking for intelligent vehicles," *Trans. Intell. Veh.*, vol. 6, no. 3, pp. 513–522, 2020.
- [14] J. Reeds and L. Shepp, "Optimal paths for a car that goes both forwards and backwards," *Pacific J. Math.*, vol. 145, no. 2, pp. 367–393, 1990.
- [15] D. Dolgov, S. Thrun, M. Montemerlo, and J. Diebel, "Practical search techniques in path planning for autonomous driving," *Ann Arbor*, vol. 1001, no. 48105, pp. 18–80, 2008.
- [16] S. Zhang, Z. Jian, X. Deng, S. Chen, Z. Nan, and N. Zheng, "Hierarchical motion planning for autonomous driving in large-scale complex scenarios," *IEEE Trans. Intell. Transp. Syst.*, vol. 23, no. 8, pp. 13 291–13 305, 2021.
- [17] S. Zhang, Y. Chen, S. Chen, and N. Zheng, "Hybrid a-based curvature continuous path planning in complex dynamic environments," in *IEEE Intell. Trans. Syst. Conf.*, 2019, pp. 1468–1474.
- [18] A. Scheuer and T. Fraichard, "Continuous-curvature path planning for car-like vehicles," in *Proc. IEEE/RSJ Int. Conf. Intell. Robots Syst.*, 1997, pp. 997–1003.
- [19] D. González, J. Pérez, R. Lattarulo, V. Milanés, and F. Nashashibi, "Continuous curvature planning with obstacle avoidance capabilities in urban scenarios," in *IEEE Intell. Trans. Syst. Conf.*, 2014, pp. 1430–1435.
- [20] M. Abramowitz and I. A. Stegun, "Handbook of mathematical functions with formulas, graphs and mathematical tables," *New York: Dover*, 1968.
- [21] M. Brezak and I. Petrović, "Real-time approximation of clothoids with bounded error for path planning applications," *IEEE Trans. Robot.*, vol. 30, no. 2, pp. 507–515, 2013.
- [22] L. Wang, K. T. Miura, E. Nakamae, T. Yamamoto, and T. J. Wang, "An approximation approach of the clothoid curve defined in the interval $[0, \pi/2]$ and its offset by free-form curves," *Comput. Aided Des.*, vol. 33, no. 14, pp. 1049–1058, 2001.
- [23] H. Yang and M. Wu, "python motion planning," https://github.com/ai-winter/python_motion_planning, 2024, [Online]. Accessed: 2024, master branch.